Nuclear Instruments and Methods in Physics Research A 782 (2015) 149–158

Contents lists available at ScienceDirect

Nuclear Instruments and Methods in Physics Research A

journal homepage: www.elsevier.com/locate/nima

In situ radiation test of silicon and diamond detectors operating in superfluid helium and developed for beam loss monitoring

C. Kurfürst [a], B. Dehning [a], M. Sapinski [a], M.R. Bartosik [a], T. Eisel [a], C. Fabjan [a], C.A. Rementeria [a], E. Griesmayer [b], V. Eremin [c], E. Verbitskaya [c,*], A. Zabrodskii [c], N. Fadeeva [c], Y. Tuboltsev [c], I. Eremin [c], N. Egorov [d], J. Härkönen [e], P. Luukka [e], E. Tuominen [e]

[a] CERN, Geneva, Switzerland
[b] CIVIDEC Instrumentation, GmbH, Vienna, Austria
[c] Ioffe Institute, St. Petersburg, Russian Federation
[d] Research Institute of Material Science and Technology, Zelenograd, Moscow, Russian Federation
[e] Helsinki Institute of Physics, Helsinki, Finland

ARTICLE INFO

Article history:
Received 15 October 2014
Received in revised form
22 January 2015
Accepted 1 February 2015
Available online 7 February 2015

Keywords:
Large hadron collider
Beam loss monitoring
Radiation hardness
Silicon detector
Single-crystal diamond detector
Liquid helium

ABSTRACT

As a result of the foreseen increase in the luminosity of the Large Hadron Collider, the discrimination between the collision products and possible magnet quench-provoking beam losses of the primary proton beams is becoming more critical for safe accelerator operation. We report the results of ongoing research efforts targeting the upgrading of the monitoring system by exploiting Beam Loss Monitor detectors based on semiconductors located as close as possible to the superconducting coils of the triplet magnets. In practice, this means that the detectors will have to be immersed in superfluid helium inside the cold mass and operate at 1.9 K. Additionally, the monitoring system is expected to survive 20 years of LHC operation, resulting in an estimated radiation fluence of 1×10^{16} proton/cm^2, which corresponds to a dose of about 2 MGy. In this study, we monitored the signal degradation during the *in situ* irradiation when silicon and single-crystal diamond detectors were situated in the liquid/superfluid helium and the dependences of the collected charge on fluence and bias voltage were obtained. It is shown that diamond and silicon detectors can operate at 1.9 K after 1×10^{16} p/cm^2 irradiation required for application as BLMs, while the rate of the signal degradation was larger in silicon detectors than in the diamond ones. For Si detectors this rate was controlled mainly by the operational mode, being larger at forward bias voltage.

1. Introduction

The superconducting magnets of the Large Hadron Collider (LHC) located close (within a few tens of meters) to the Interaction Points (IP) of the proton beams are exposed to high-radiation fields due to the collision debris. The Beam Loss Monitoring (BLM) system is an integral component of the LHC, which measures the particle showers from beam losses. BLM signals which exceed the protection thresholds trigger the beam abort system. By these means the quench of the superconducting magnet coils can be prevented and various LHC components are protected from damage. The sensitivity of the monitors depends on their location and orientation with respect to the beam. It has been shown using Fluka simulation [1] that with the present configuration of the BLMs installed outside the cryostats of the final focusing triplet magnets, the ability to measure energy deposition into the magnet coils is limited because of the collision debris, which mask the beam loss signals. This is illustrated in Fig. 1, where the signals in the BLM sensors are shown for cases of beam debris and the occurrence of a quench-provoking beam loss. At the top of the figure the location of magnets Q1–Q3 and BLMs is visualized, with the BLMs placed inside or outside the ring, giving signals with a small difference. As a result of the proximity of the interaction point, differentiation between the signals from the quench-provoking beam losses and from the continuous collision debris is difficult.

There is an ongoing activity that started in 2011 to upgrade the BLM systems of the LHC by installing the sensors inside the cold mass, as close as possible to the superconducting coils. The direct advantage of cryogenic BLMs (CryoBLMs) would be that the measured dose corresponds more precisely to the dose deposited into the coil. The main requirements for CryoBLMs are listed below:

* Corresponding author. Tel.: +7 812 292 7953; fax: +7 812 297 1017.
E-mail address: elena.verbitskaya@cern.ch (E. Verbitskaya).

http://dx.doi.org/10.1016/j.nima.2015.02.002
0168-9002/

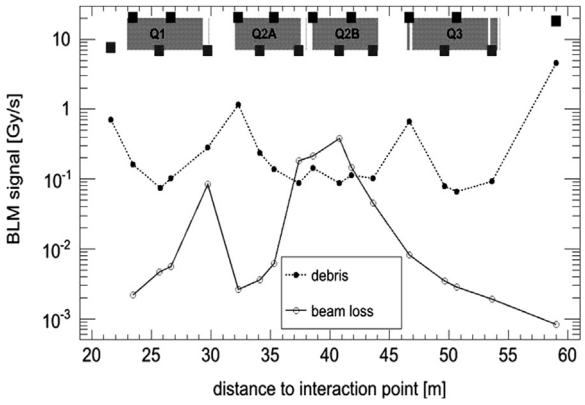

Fig. 1. BLM signal from debris and from quench-provoking beam losses (one point for each BLM) in the inner triplet region of the LHC. At the top the locations of the magnets (Q1–Q3) and BLMs (small boxes) are visualized.

1. A low operational temperature of 1.9 K (superfluid helium).
2. An integrated dose of about 2 MGy (in 20 years, without accidents).
3. The detector response should be linear between 0.1 and 10 mGy/s, which is the range of signals expected close to the quench, and faster than 1 ms.
4. The CryoBLM sensors should work in a magnetic field of 2 T and at a pressure of 1.1 bar, withstanding a fast rise in pressure up to about 20 bar.
5. Once the detectors have been installed into the LHC, no access will be possible; therefore the detectors need to be reliable and stable for 20 years.
6. A predictable rate of the sensitivity degradation with a minimal deviation over a large number of sensors, which should be guaranteed by the sensor processing and calculated from the parameters of the sensor material and construction (dimensions and technology).

Two types of BLM radiation detectors based on either silicon or diamond material are currently under investigation. Radiation detectors made of silicon are cost-effective due to application of industrial planar technology. Their radiation hardness properties at room temperature (*RT*) and insignificant cooling are rather well known because of the numerous investigations of the CERN-RD50 collaboration ([2,3]) and they are widely used for tracking of charged particles in high-energy physics experiments.

The advantage of diamond detectors with regard to radiation hardness arises from the wide bandgap of diamond and the higher displacement energy, plus higher carrier mobility [4]. Therefore the dark current is almost negligible, even at *RT*, and no active cooling is needed. This makes it possible to build fast and low-noise charged particle diamond detectors [5–7] which are a very favorable option for a smaller scale or unique applications of single devices such as radiation monitoring at certain points of the LHC experiments, or in which it is impossible to construct an active cooling system. Recently, diamond detectors were tested in the collimation area of the CERN LHC to study their feasibility as Fast Beam Loss Monitors in a high-radiation environment [8,9]. However, the large electron–hole pair creation energy in diamond material leads to a reduced signal compared with silicon of equal thickness and energy of minimum ionizing particles (MIP).

The first beam test of nonirradiated semiconductor prototypes of BLM sensors was performed at LHe temperature at CERN in the Proton Synchrotron (PS) beam line T9 [10,11]. All the detectors that were tested proved to be operational in direct current (DC) and single-particle counting (AC) modes when placed at $\sim$2 K. In addition to overall functionality at very low temperatures, the next important issue to be addressed is the radiation hardness of silicon and diamond detectors under the operational conditions of BLMs. Earlier the characteristics of irradiated Si detectors at temperatures in the range from 77 K to *RT* were investigated to explain the so-called "Lazarus effect" [12]. It was shown that the recovery of the signal occurred at $T\sim$180 K in detectors irradiated at *RT*, which was not affected by the temperature of irradiation (*RT* and 85 K were tested) or by reverse annealing [13]. It was demonstrated that the origin of the temporary recovery of the detector sensitivity is the change in the occupancy of radiation-induced trapping centers by electrons and holes, which is not stable over time and therefore is not an issue for the improvement of the detector radiation hardness.

From the physics of radiation defect formation it is expected that radiation damage on semiconductor materials can be substantially different at the LHe temperature compared to *RT* and even at the temperature of liquid nitrogen. For example, at such low temperatures the reduced migration of primary defects, interstitials and especially vacancies [14,15] may change the radiation defect energy level spectrum and affect the properties of carrier capture and emission. Reverse annealing, which is one of the main causes of radiation degradation of Si detectors around *RT*, would be significantly reduced or even ceased completely.

The first *in situ* irradiation test at 1.9 K of Si and diamond detectors developed for CryoBLMs was performed at CERN during November and December 2012, and its description and experimental data were presented in fragments in Refs. [11,16–18]. The detectors were installed inside a liquid helium cryostat while being irradiated *in situ* by 24 GeV/c protons provided by the CERN PS accelerator. This test beam experiment is particularly unique because of the very low temperature of 1.9 K and high integrated radiation dose of up to 2 MGy. The main task of this study is gaining insight into the radiation hardness of Si and diamond detectors at such a low temperature and verifying that the detectors can operate under the conditions listed above in points 1 and 2 required for semiconductor CryoBLMs. The overall description of the experiment, its results and qualitative analysis are reported taking into account the physics of semiconductor detector operation under irradiation.

2. Experimental setup and procedures

Irradiation campaigns at *RT* (or around) are usually carried out in steps, namely, the samples are first irradiated to the desired fluence *F* and then brought, under temperature- and time controlled conditions, into a laboratory for characterization. After the measurements, the samples might be returned into the irradiation for the next step, and the thermal history of the samples is recorded. In the case of the experiment at liquid helium temperature this is, however, not possible (unless the beam can be stopped) since warming-up the samples even to 80 K can result in significant defect annealing and, thus, misleading conclusions about the physical properties of the irradiated material and the sensors. Therefore cryogenic irradiation test must be performed as *in situ* test with the measurements carried out permanently using a special cryostat and proper cabling.

2.1. Irradiation

The cryogenic *in situ* irradiation test was performed at PS East Hall (T7 experimental area) at CERN during November and December 2012. The energy of the proton beam was 23 GeV and the full width at half-maximum of the beam diameter was tuned to be about 1 cm at the detector location. The beam intensity was 1.3×10^{11} proton/cm^2 per 400 ms spill, corresponding to about 1×10^{10} proton/s on the detectors and the planned maximum fluence of 1×10^{16} proton/cm^2 was reached. The fluence and the

total dose in the radiation facility were well-controlled parameters during and after the irradiation with the accuracy of ±7% [19,20].

2.2. Cryogenic system

The cryogenic system was especially adapted to match the requirements of the radiation test facility. The main elements of the cryogenic system are the cryostat, the helium storage Dewar, the transfer line which connects the two of them and the vacuum pump (Fig. 2). The cryostat and the transfer line are also superinsulated, so that the helium can stay in a liquid state during transfer, and the boil-off rate of the helium inside the cryostat is as low as possible. The transfer line, constructed at the CERN Cryolab, supplies liquid helium to the cryostat and simultaneously transports the cold gas out of the radiated area. It consists of two concentric flexible stainless steel tubes which are vacuum-jacketed and lined with multilayer insulation. The length of the transfer line is 12 m, and it spans the distance between the cryostat located in the radiation area and the Dewar. The latter remains outside the activated zone with the rest of the vacuum equipment, such as the pump and the helium gas bottle. The temperature of the helium bath was lowered from 4.2 K to 1.9 K by pumping off the transfer line decoupled from the storage Dewar by the valve.

The cryostat was periodically filled with LHe from the storage Dewar (once per 24 h) and during this procedure the temperature increased to 4.2 K. Thus, the temperature of the samples was 1.9–4 K within 95% of the irradiation campaign time. No significant difference of the detector properties within this temperature range was observed. Towards the end of the irradiation, a warm-up cycle up to 80 K was performed to simulate the thermal history of the winter technical stop of the LHC and its influence on the detector properties when the cold mass of the magnets is warmed up to this temperature.

Finally, the last two days of a five-week irradiation campaign were utilized to warm the detectors up to room temperature and simultaneously measure the temperature dependence of the characteristics of the detectors that were investigated.

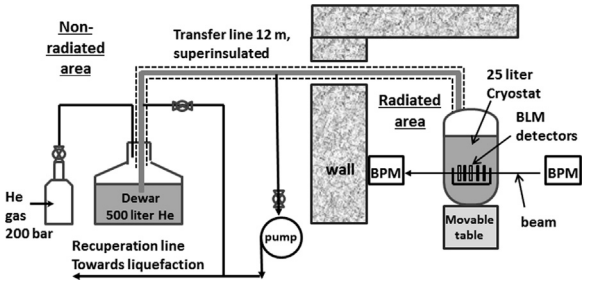

Fig. 2. A simplified schematic of the cryogenic instrumentation and irradiation. BPM—beam position monitor.

Table 1
Characteristics of the detectors under study.

	Material	Resistivity (Ω cm)	Thickness (μm)	Sensitive area (mm^2)	V_{fd} at RT (V)	Measurements
1	Silicon 1	10^4	300	5 × 5	33	I–V, Q_c
2	Silicon 1	10^4	300	1 × 1	33	Pulse signal
3	Silicon 2	500	300	5 × 5	670	I–V, Q_c
4	Silicon 3	4.5	300	5 × 5	$\gg 10^3$	I–V, Q_c
5	Diamond 1	Undoped	500	4 × 4		I–V, Q_c
6	Diamond 2	Undoped	500	4 × 4		I–V, Q_c

2.3. Semiconductor detectors

p+/n/n+ Silicon pad detectors were designed and processed by the Ioffe Institute, St. Petersburg, and Research Institute of Material Science and Technology, Zelenograd, both in Russia, on wafers with different resistivity. The samples under investigation were diodes processed on silicon with a resistivity of 10 kΩ cm, 500 Ω cm and 4.5 Ω cm, with aluminum metallization. The thickness of all silicon samples was 300 μm. The full depleted voltage V_{fd} was estimated in accordance with the Si resistivity.

In addition to the silicon detectors, two single-crystal diamond detectors were investigated. The diamond samples were made of single-crystal chemical vapor deposition (sCVD) 500 μm thick substrates. The detectors were produced by CIVIDEC Instrumentation, GmbH, Austria [5]. The metal contacts were gold and titanium adhesion layers with platinum in-between. The parameters of the detector samples are specified in Table 1.

2.4. Detector modules and silicon beam telescope

To organize different types of detectors for testing and to realize their various operational modes, different types of holders were used (see Figs. 3–5 in [16]). The holders for the DC measurements integrated two rigid stainless steel cryogenic coaxial cables and a detector mounted on the metalized pad electrically insulated from the ground. This type of holder was used for one silicon and two diamond detectors and corresponded totally to the schematic of the signal readout from the detectors in the developed BLM system. In this arrangement the bias voltage was applied directly to the detector n^+ side (the back side), and the current meter measured the current between the p^+ contact and the ground.

In the holders for fast signal readout the back n^+ contact of Si detector was grounded, and only one cable was used for both the signal readout and biasing. This simplified arrangement was optimal for the measurements using the Transient Current Technique (TCT) [21], for which the holders contained a compact rectangular mirror tilted 45° with respect to the detector surface and an optical fiber to send a short (< 50 ps) laser pulse to the mirror which reflected it to the detector p^+ side. Among five holders of this type, one allowed the illumination of both sides of the detector (2 in Table 1). The holders with silicon and diamond detectors were put together as a stack and attached to the copper

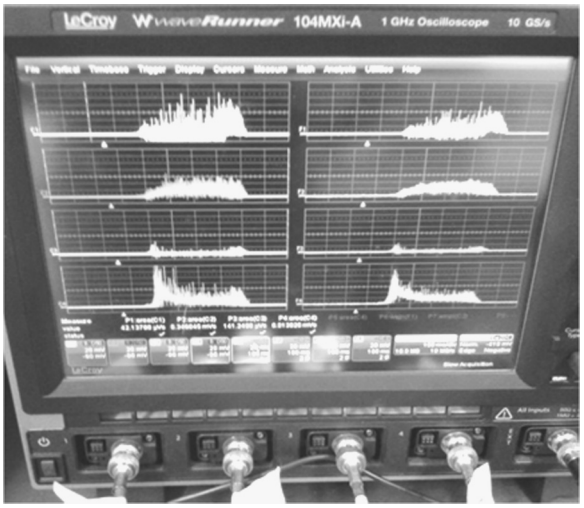

Fig. 3. The signals from four detectors of the silicon beam telescope used in the beam alignment: left—single pulse measurements, right—averaging of 10 pulses. Here the difference in the signal amplitudes indicates that the beam axis is shifted towards one of the detectors.

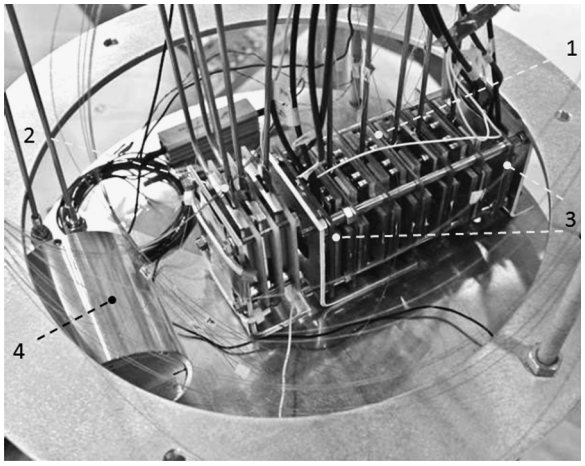

Fig. 4. Detector solid module with the attached beam telescopes mounted on the plate and ready for cooling and irradiating. 1 and 2 – holders with Si and diamond detectors, respectively, 3 – silicon beam telescopes, 4 – Secondary Emission Chamber.

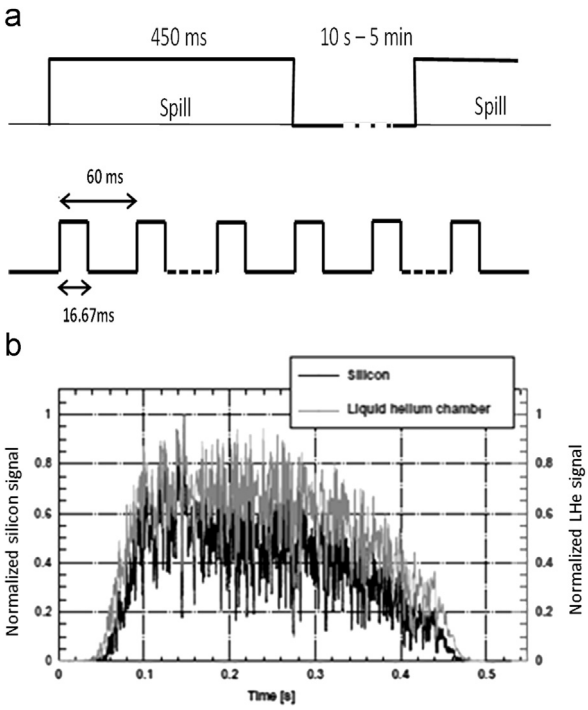

Fig. 5. Time diagram of the DC current and collected charge measurements (a), and the shape of a spill recorded by Secondary Emission Chamber and by one of the silicon detectors of the beam telescopes (b).

plate on the bottom of the cryostat as a solid detector module. As follows from Table 1, six detectors from all those installed were used in the measurements.

Particular attention was given to the best possible alignment of the detectors inside the cryostat with respect to the proton beam. The contraction in the length of the rods holding the copper plate caused by cooling from *RT* to the LHe temperature was taken into account when placing the cryostat for irradiation. For the permanent control of the beam, two beam position monitors (BPM) were installed outside the cryostat (Fig. 2), which measured the intensity and the profile of the beam and its position at all time and for each spill. The first alignment of the beam after installation of the cryostat in the irradiation zone was performed prior to irradiation and visually with a laser.

A permanent control of the beam position with respect to the detectors in the *in situ* irradiation was carried out using two silicon beam telescope modules. The telescope modules contained four silicon detectors each, mounted tightly together as quadrants. In total, eight silicon detectors from the beam telescopes were connected to the same voltage at the n^+ side. The front side (p^+ contact) of each Si detector was directly connected through a standard CB-50 cable to a 1 GHz LeCroy oscilloscope, so it was possible to readout independent signals generated by spill from each detector. The signals from one of the beam telescopes are shown in Fig. 3. Two holders with the beam telescopes were located at both outer positions of the detector solid module installed inside the cryostat (Fig. 4). Comparison of the DC signals from eight detectors gave the information for the initial tuning of the beam position and allowed the alignment to be verified. The criterion for a correct alignment was a symmetric distribution of the current signals with close amplitudes between the quadrants in both the input and output telescope detectors, which was stable in a long-term scale of the experiment, although there were some short-term shifts of the beam position (Fig. 3).

The solid detector module with the attached beam telescopes arranged on the ground plate and ready for installation inside the cryostat is shown in Fig. 4. At the outer extremities of the detectors aluminum foils were placed to confirm the total dose at the end of the irradiation. A Secondary Emission Chamber (SEC), which is actually a liquid helium chamber, installed inside the cryostat was used for the on-line control and calibration of the fluence.

The bias voltage could be set between −400 V and +400 V for all the detectors, which allows the operation of silicon detectors from the reverse bias mode to the forward bias mode; the latter corresponds to a Current Injected Detector (CID) [22].

2.5. Measurement of the collected charge

The collected charge Q_c was determined by integrating the detector output current over the 400 ms spill. The measurements of the direct current and detector biasing were performed using a Keithley 6517 source meter unit (SMU). The SMU was controlled by means of the LabVieW data acquisition program over a GPIB remote connection.

A time diagram of the DC current and collected charge measurements is shown in Fig. 5a. The number of power line cycles of the current measurements corresponded to 16.67 ms, meaning that the recorded current value was the averaged current over 16.67 ms. The duration of the spills was typically between 400 and 470 ms. One measurement point was taken each 60 ms. This sampling rate was limited by the structure of the LabVieW program and the time needed to send and receive the messages between the PC and the Keithley instrument through the GPIB connection. The time between the spills could be between 10 s and 5 min, depending on the performance of the machine and on the number of spills that arrived within a supercycle. Each spill had a unique shape (Fig. 5b), but some systematic parts within the spill with more or less intensity could be observed. As the measurements of the detector signals were not synchronized with the arrivals of the spills, which were randomly distributed in time, we avoided a systematic error in the measured current. The current coming from the detector was integrated and, hence, the charge per spill was obtained (using a linear interpolation between the measurement points within a spill). To get one point of the results described in Sections 3.2 and 3.3, a minimum number of 20 spills were recorded to get an averaged value of the charge collected in the detector.

However, statistics of the charges collected from the individual spills showed significant deviations from its averaged value, which could not be attributed to the nonsynchronized measurement procedure mentioned above. This indicates existing of the additional source of deviations, which can come from nonuniformity of

the proton density inside the beam, or deviations of its position visualized by the Si beam telescopes (Fig. 3) and BPMs. Thus, despite the averaging of the DC signals over 20 spills, these factors are presumably responsible for rather large statistical errors of about $\pm$15% of the obtained charge.

Then the obtained charge was normalized to the number of incident protons to get the collected charge as a charge per MIP [11]. This number was extracted from the signals of SEC, which were integrated in a dedicated circuit over a spill time and encoded in a pulse sequence by a charge–frequency converter. The sequence was sent to the counter (Agilent 53131A, a 225 MHz bandwidth) to determine the number of pulses proportional to the amount of protons. The proportionality factor was derived from the final irradiation fluence measured by the aluminum foil at the end of the *in situ* test. The foil was aligned with the detectors (placed on the axis of the detectors), and its area was equal to the Si detector area.

2.6. Measurement of TCT signal

The TCT measurement readout was made using a 20 dB amplifier from CIVIDEC to increase the signals coming from the silicon detectors. The acquisition of the pulse response was carried out with a LeCroy WavePro 7300A oscilloscope with a 3 GHz analog bandwidth, which was triggered by a picosecond laser. The laser light was generated by a PiLas Digital Control Unit (EIG1000D) and an optical head for a 630 nm wavelength. Special radiation-hard optical fibers immersed in liquid helium were used.

3. Experimental results

3.1. I–V characteristics

The *I–V* characteristics of the nonirradiated Si detectors at *RT* had a shape typical for $p^+/i/n^+$ diodes. In the reverse bias mode the current had the tendency to saturate at a value in the range of nA (with the exception of the 4.5 Ω cm sample, whose full depletion voltage V_{fd} was far above 1 kV (Table 1), which prevents full depletion from being achieved). At forward bias V_{forw} the current rose sharply at a low bias voltage. For the diamond detectors with a symmetric metal-insulator-metal structure, a linear ohmic-like behavior was observed in both polarities with a current in the range of tens of pA. Such a small current was still higher than the leakage current of the connecting cables (about 1 pA), which implies the current flowed through the Au-diamond interfaces and along the surface of the chip edge.

After cooling down to 1.9 K, the current of the Si detectors operating at reverse bias V_{rev} dropped and was in the pA range. In opposite polarity the forward current exposed the same rising behavior, which indicates effective hole injection from the p^+ contact into the silicon n-type bulk. The *I–V* characteristics of the diamond detectors did not change much keeping an ohmic behavior and the same current values.

After *in situ* irradiation to the fluence of 1×10^{16} p/cm^2 at 1.9 K, the *I–V* characteristics changed their shape in both the Si and diamond detectors. In Si detectors the current decreased to below 100 pA and the shapes of the *I–V* curves became similar in both polarities (Fig. 6a).

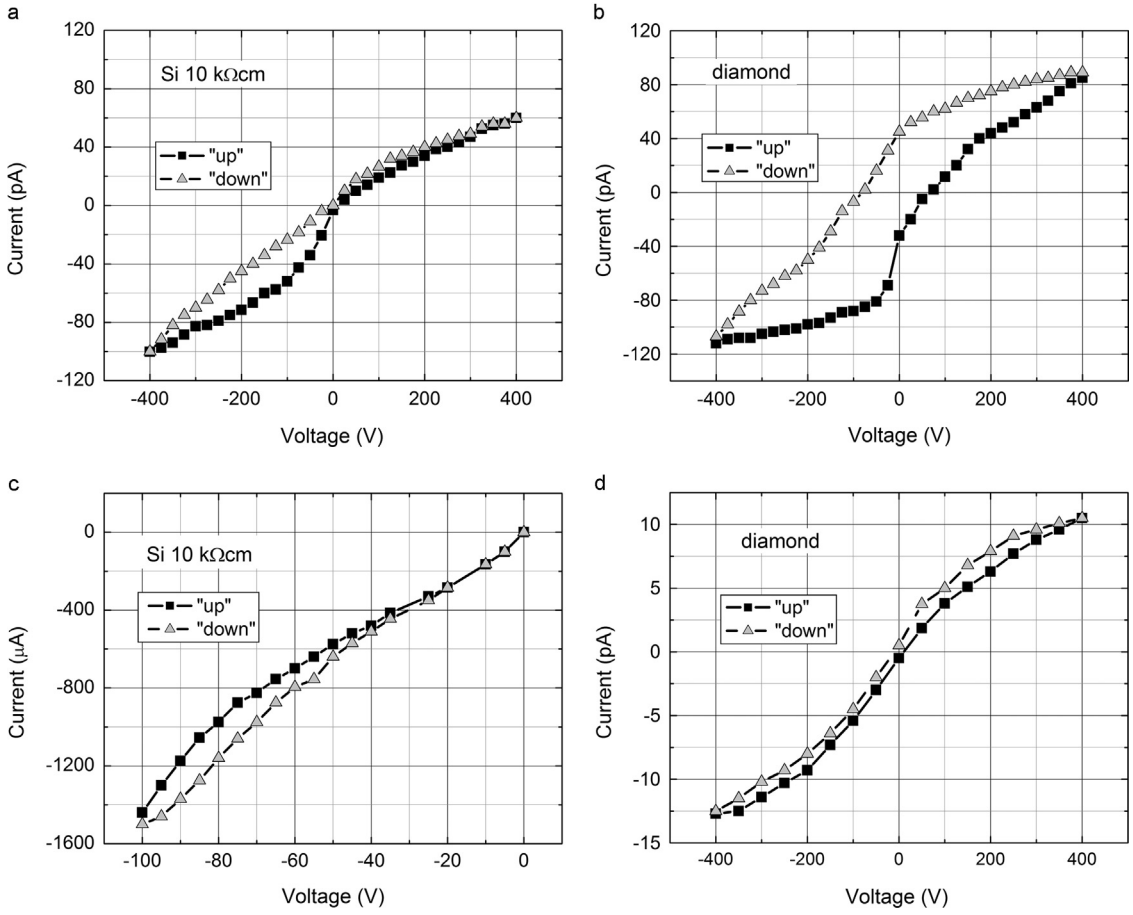

Fig. 6. *I–V* characteristics of irradiated Si and diamond detectors at 1.9 K (a and b) and after heating to *RT* (c and d). *F* (p/cm^2): a and b – 1×10^{16}; c and d – $\sim 1.2 \times 10^{16}$. The terms "up" and "down" correspond to the measurements of the *I–V* characteristics at a fixed temperature when the bias voltage increases (run "up") or goes down (run "down").

However, the slope was about two times lower for the forward current compared with that for the reverse one. This is a clear indication that the current in the reverse and forward bias modes is still controlled by different mechanisms. A lower density of the forward current can indicate high efficiency of the Space Charge Limited Current (SCLC) mechanism [23] at very low *T*. However, the important feature of SCLC, a sharp current rise, is not observed at forward bias up to 400 V. Such behavior qualitatively correlates to the model of the Current Injected Detectors [22]. According to this model, in heavily irradiated Si detectors current injection is limited by the trapping of injected carriers on the deep levels of radiation-induced defects in the detector bulk, and the current decreases with the accumulated fluence and reduction of the temperature. As soon as all the deep traps are filled with the captured carriers, the current immediately exhibits a steep rise, which happens in the range of hundreds of volts at a fluence of around 1×10^{15} p/cm^2 and *T* around 220 K. This rise is not observed in the experimental *I–V* curves in Fig. 6a, which indicates a significantly higher density of active trapping centers in Si detectors irradiated in LHe compared with *RT* irradiation.

Irradiation at 1.9 K did not affect the current in the diamond detectors; it remained in the range of tens of pA even if the fluence was 1×10^{16} p/cm^2 (Fig. 6b). However, its non-ohmic shape became more pronounced. The observed hysteresis in the bias runs "up" (increasing bias) and "down" (decreasing bias) at LHe is evidence of polarization. This effect is specific for the detectors with a metal-semiconductor-metal based structure on the materials, in whose bulk the concentration of trapping centers with deep energy levels is high. These centers may be intrinsic defects in wide-bandgap semiconductors (like in *e.g.* CdTe [24]) or radiation-induced defects. In detectors operating at low *T* capture of free carriers on deep levels prevails over emission, which causes accumulation in time of the charge somewhere inside the bulk and the redistribution of the potential and electric field profile such as appearance of a high resistivity electrically neutral base region. These effects lead to the degradation of the detector sensitivity (signal) as was observed in irradiated Si detectors [25].

In the measurements of *I–V* characteristics of the diamond detectors the change of the current with the bias depends on the rate of carrier transfer through the metal-diamond barriers. This rate can be misbalanced with the current flow through the detector bulk and the rate of the bias voltage scan, which leads to hysteresis in the bias "up" and "down" runs in the diamond detector. This effect is very small in the Si detectors operating at V_{rev} (Fig. 6a) and quite negligible in the CID mode since in the latter case carrier injection encourages the disappearance of the accumulated charge.

The final heating of the samples to *RT* was carried out under irradiation reaching an accumulated fluence of 1.16×10^{16} and 1.22×10^{16} p/cm^2 in the Si and diamond detectors, respectively. It led to an increase in the reverse current up to 1.5 mA in Si irradiated detectors (Fig. 6c), whereas the curves showed a sharp rise at forward bias (not displayed in the figure). Heating also eliminated hysteresis in the bias "up" and "down" runs of the diamond detector (Fig. 6d), and the current became lower than at 1.9 K.

It should be noticed that the *I–V* characteristics at LHe temperature (Fig. 6a and b) have a curtain structure, and therefore they cannot be definitely assigned to the leakage. Different mechanisms are evinced in the curves of the Si detectors; in the forward bias mode it is SCLC, while at reverse bias it is a carrier flow across the p^+–n junction barrier and probably the additional current generated in the high-doped p^+ layer. In the diamond detectors these mechanisms are even more pronounced and, additionally, they interfere with the polarization effects related to the defects of crystal lattice and radiation-induced defects, which may change the barriers near the metal-diamond interface and, consequently, the mechanism of the current flow. The latter assumption agrees with the fact that the current of the diamond detectors is lower at *RT* than that at 1.9 K. However, the reasons for these effects in the diamond detectors are not yet clear and need special study.

3.2. Dependences of the collected charge on fluence

The critical parameter for the BLM semiconductor detectors is their sensitivity at the expected maximum accumulated fluence. To simulate the detector performance over several years of non-stop operation in the experiments, the same maximum fluence was achieved in the *in situ* irradiation test during five weeks. Obviously, the mean intensity during the irradiation was higher than in the case of LHC operation. However, an increase in the proton beam intensity by a factor of up to 50 allows the operation of the detectors to be tested under conditions close to those which can appear during the quench-provoking events at the LHC.

The detectors under irradiation were permanently connected with the current meter in such a way that the current generated by spills was recorded as a function of the accumulated fluence. The results in terms of the detector sensitivity are presented as the charge Q_c collected from a single detected MIP, which allows comparison of the detector sensitivity with the results presented in numerous publications on the radiation hardness of semiconductor detectors at *RT*. For the analysis the results were grouped into two sets: the $Q_c(F)$ and $Q_c(V)$ dependences for the standard reverse biased Si detectors and the same detectors operated as CIDs, and for the diamond detectors whose signal was the same at both polarities because of their symmetric structure, and in the $Q_c(F)$ curves it is presented as a charge recorded at positive bias only. In the measurements the maximum bias voltage was limited by the value of ±400 V, which is the expected operational bias for BLMs and allows the application of special materials and electrical components to be excluded. In the figures presented in Sections 3.2 and 3.3 the $Q_c(F)$ dependences are shown in the range 10^{14}–10^{16} p/cm^2, which corresponds to the fluences of the main interest.

The set of $Q_c(F)$ characteristics for detectors processed on 10 kΩ cm and 500 Ω cm silicon is depicted in Fig. 7a–d, at different bias voltages. The data are presented in log/log scale, and in the above-mentioned fluence range almost all the curves demonstrated a decay of the charge with a slope around -1 and -0.5 at forward and reverse bias voltage, respectively. In the latter case (Fig. 7a) the collected charge increased when the absolute value of the bias rose from 50 to 100 V and then was less sensitive to the growth of the absolute value of the bias up to 400 V. The measurements of the *I–V* characteristics showed that in CIDs irradiated to low *F* (below 1×10^{14} p/cm^2) the forward current was about 100 μA at 100 V even in liquid helium, which exceeds the signal from the spills and gives an incorrect value of the collected charge. To reach a lower current and efficient charge collection, the concentration of traps arising from radiation-induced defects in the silicon bulk should be accumulated, which is realized at a fluence around 5×10^{14} p/cm^2. The current decreased to a value below 60 pA and no sharp rise was observed anymore. The growth of the collected charge with the bias voltage increase was more gradual (Fig. 7b) than that in the case of a reverse-biased detector. Such behavior of silicon CIDs correlates with the fundamental features of SCLC in deep-level rich semiconductors, which was explained in detail in [22,23]. In the range of medium $F\sim(1–3)\times10^{15}$ p/cm^2 the charge collected in the forward-biased detector irradiated to the same fluence became larger than that at V_{rev} (Fig. 7f, below), and the dependences were well approximated by the Q_c *vs.* F^{-1} function.

Similar features were observed for the degradation of the collected charge in the detector processed on 500 Ω cm Si (Fig. 7c and d) and even in the detector processed on 4.5 Ω cm

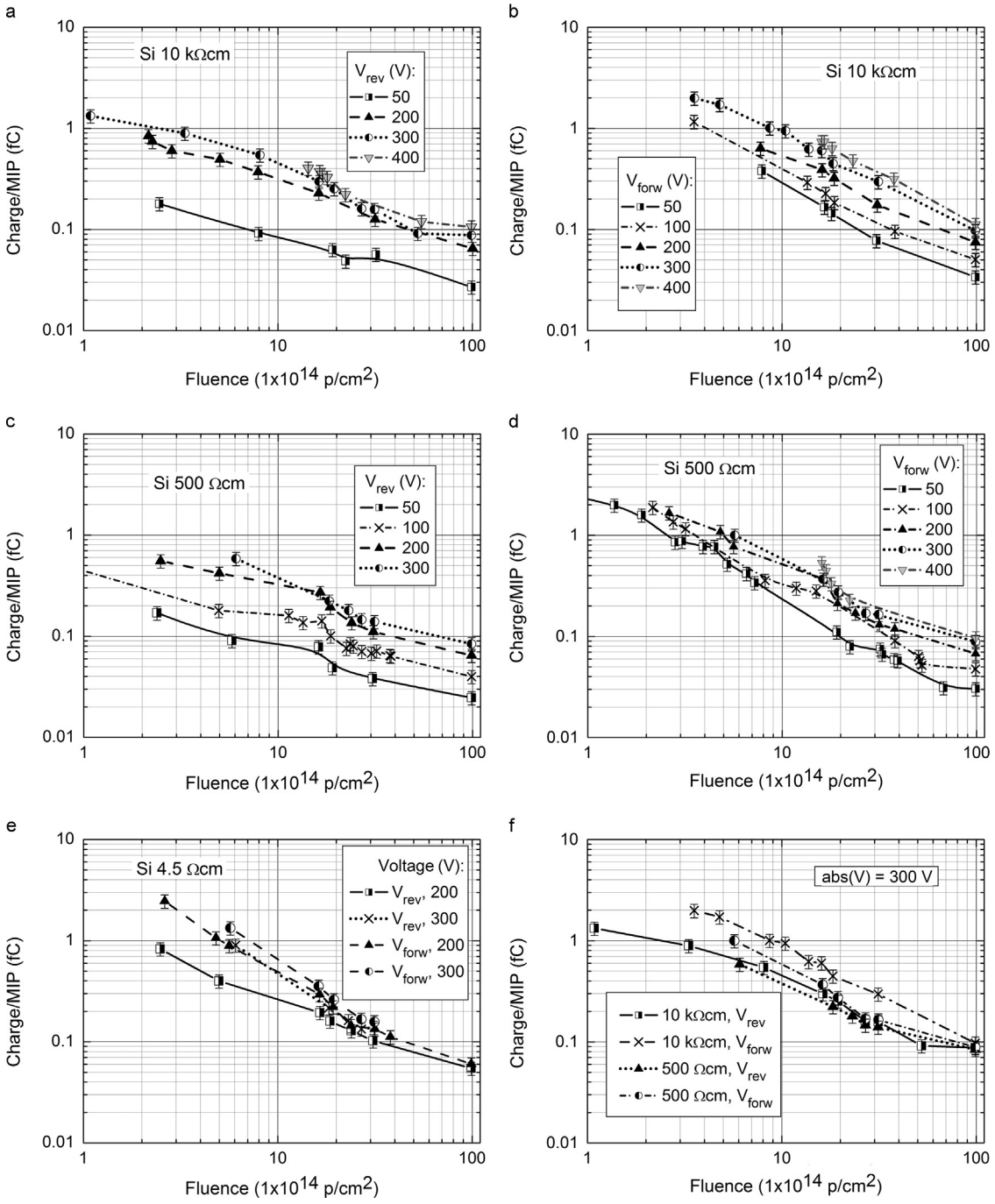

Fig. 7. Dependences of the collected charge *vs.* fluence in Si detectors at different bias voltages and polarity of the bias (a–e), and comparison of 10 kΩ cm and 500 Ω cm Si detectors operating at different bias polarity (f). $T=1.9$ K.

Si operating at $V_{rev}=200$–300 V (Fig. 7e). Evidently, at a lower fluence the charge collected in the detectors operating as CIDs was larger than Q_c at the reverse bias, whereas the decay of the $Q_c(F)$ dependences was less pronounced at the reverse bias, which may be related to the field effects. The remarkable feature is that at the highest fluence, of 1×10^{16} p/cm^2, the collected charge is insensitive to the silicon resistivity and practically the same at both polarities of the voltage (Fig. 7f).

The decreases in the signal with increased proton fluence for the diamond detectors and a comparison between the detectors at $V=\pm400$ V, the latter is given in the range 1×10^{15}–1×10^{16} p/cm^2, are depicted in Fig. 8a and b, respectively. At the final fluence the charge collected in the diamond detector is 40% larger than that in the Si detector processed on 10 kΩ cm Si. Preliminary estimations showed that the rate of degradation of the collected charge in the Si detectors at 1.9 K was higher than at *RT*.

3.3. Dependences of the collected charge on bias voltage

The dependences of the collected charge on the bias voltage (voltage scans) are presented for all detectors in Figs. 9 and 10 at both polarities of the bias voltage. In the scans of the Si detectors whose structure is asymmetrical positive voltage denotes forward bias. For the diamond detector both positive and negative branches were nearly identical due to its symmetric structure. For all the types of detectors and operational modes the signal

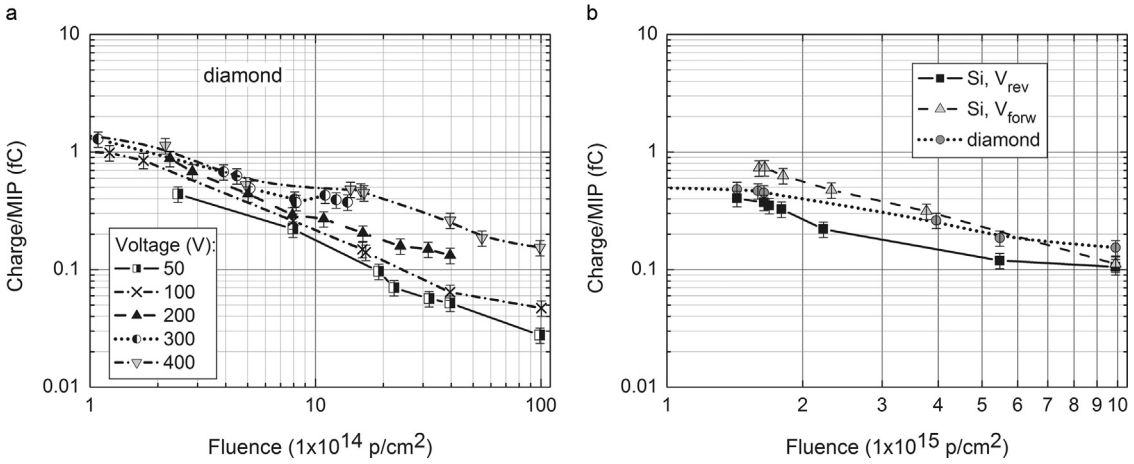

Fig. 8. Dependences of the collected charge *vs.* fluence in diamond detectors at different bias voltage (a), and comparison between 10 kΩ cm silicon and diamond detectors operating at ±400 V (b).

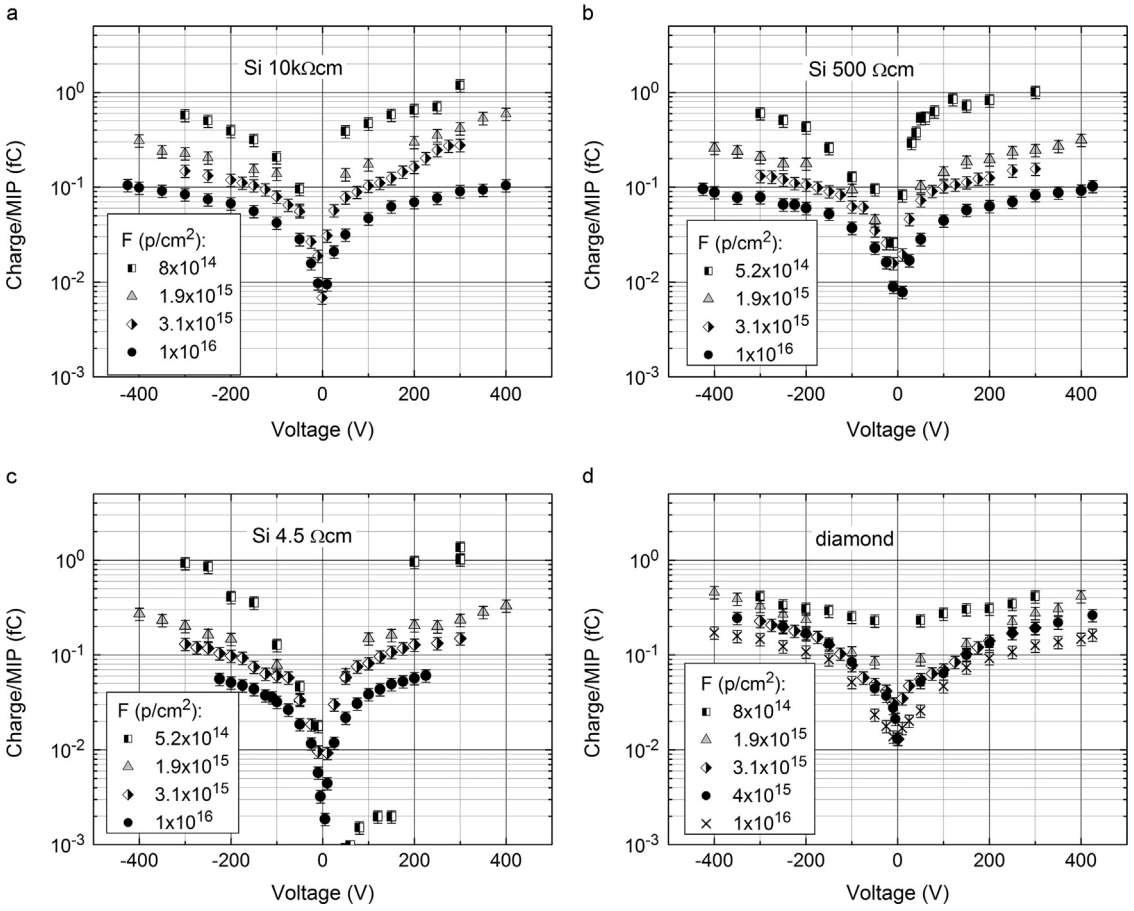

Fig. 9. Dependences of the collected charge on bias voltage in Si (a–c) and diamond (d) detectors irradiated to various fluences.

increased with the bias, which was especially evident at V below 200 V. In the detectors processed on 10 kΩ cm and 500 Ω cm Si the Q_c rise at the highest voltage was more pronounced at V_{forw} *i.e.* in CIDs compared with the reverse-biased detectors (Fig. 9a and b), which correlates to the curves shown in Fig. 7f.

To explain this feature, it should be noticed that the average electric field $\bar{E}=V/d$ in the bulk of heavily irradiated Si detectors has the same value in both modes and, in a rough approximation, the electric field $E(x)$ should be uniformly distributed through the detector bulk. Hence, the dependence of the drift velocity on the electric field, $v_{dr}(E)$, is a dominant factor for the collected charge and would give the rise of Q_c at lower V followed by the same value of the saturated charge, irrespective to the bias polarity. However, the distribution of the electric field in heavily irradiated Si detectors, both CIDs and reverse-biased ones, is not uniform and, moreover, has different profiles. A specific feature of CIDs is that there is a relatively narrow region with a low electric field, whose depth reduces with bias [22]. Furthermore, at the same absolute values of the bias voltage the depth of the high electric field region is larger at V_{forw}, which leads to a shift in the collected charge saturation in CIDs to a lower bias voltage and gives a higher Q_c value.

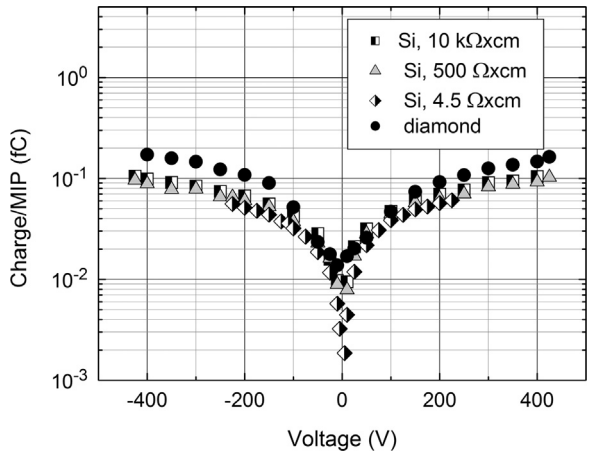

Fig. 10. Comparison of the charge collected at various bias voltages in Si detectors with different resistivity and diamond detector. $F=1\times10^{16}$ p/cm^2.

The $Q_c(V)$ curve of the 4.5 Ω cm Si detector irradiated to the lowest fluence of 4×10^{14} p/cm^2 and operating at V_{forw} showed abnormal behavior–a small Q_c at $V\leq150$ V, which increased up to the same value as in the other Si detectors at a bias above 200 V (Fig. 9c). At a fluence beyond 1×10^{15} p/cm^2 the shape of the $Q_c(V)$ dependences was practically the same as for the diodes processed on Si with a higher resistivity. All the measured $Q_c(V)$ characteristics showed a trend to saturate at a higher voltage of 300–400 V.

The $Q_c(V)$ dependences for the diamond detector are shown in Fig. 9d. There was no difference between the curves of the two diamond samples that were investigated. The charge collected in the sample irradiated to a fluence below 1×10^{15} p/cm^2 was practically insensitive to the bias voltage above 100 V. Such a "threshold" behavior in the sensitivity to the irradiation fluence is well expected for materials with an initially low trapping time constant τ_{tr}. In this case, the collected charge starts to reduce only when the trapping time constant reciprocal to the accumulated fluence [26] drops down to the value of the initial carrier lifetime τ in a nonirradiated material. In the diamond material the latter parameter is a few tens of ns [27], which is far below the $\tau\sim$ms in high resistivity Si. Therefore, in the studied diamond detector this condition is realized at $F>1\times10^{15}$ p/cm^2 when the trapping time constant starts to drop and the detector becomes sensitive to the fluence. The experiment showed that the $Q_c(V)$ dependences of these detectors irradiated to $F>1\times10^{15}$ p/cm^2 were similar to those for the Si detectors. The collected charge also increased with the bias voltage tending to saturation and had similar values irrespective of the polarity of the voltage. The voltage scans of the Si and diamond detectors irradiated to 1×10^{16} p/cm^2 are compared in Fig. 10. The rate of the charge rise with the bias voltage in the diamond detectors was different from that in the Si detectors, because of a larger thickness of the diamond (Table 1). The charge collected in the diamond detector was larger at $V\geq100$ V.

3.4. Current pulse response in Si detector irradiated at 1.9 K

Along with the measurements of DC characteristics, the current pulse response was recorded using TCT. These measurements were carried out for a single detector which was processed from 10 kΩ cm n-type Si and had an area of 1×1 mm^2 and optical windows on both sides. The light pulse signals with a width of 45 ps were supplied by a laser with a wavelength of 630 nm and *via* optical fibers placed near the p^+ and n^+ sides of the detector.

Since it was the first *in situ* radiation test at 1.9 K including the measurements of different steady-state and pulse characteristics, not all issues could be predicted in advance. The first one arises from the physics of radiation damage at low *T*. Specifically, primary vacancies are immobile at $T<70$ K, and therefore the formation of multivacancy complexes which are critical for radiation degradation in n-type Si detectors is expected to be significantly suppressed, and only primary interstitials can participate in radiation defect formation at 1.9 K [14,15]. The second issue is related to some technical features of the *in situ* experiment. In particular, two types of optical fibers were used, standard and radiation-hard ones. Only the radiation-hard fiber, which was connected to the detector n^+ side, withstood the radiation, and the pulse signals of the irradiated detector were recorded from the n^+ side only.

Similarly to the results on $Q_c(F)$ dependences obtained from the DC measurements, the rate of the pulse signal degradation derived from the TCT data was larger for the signals measured at reverse bias with respect to those at forward bias. The main results of the TCT measurements are:

- the width of the pulse of the nonirradiated detector decreased under cooling from *RT* to 1.9 K as a result of the increase in the carrier mobility;
- the rate of signal degradation was rather high for both bias polarities and the degradation was more pronounced at reverse bias;
- space charge sign inversion occurred at a relatively low fluence, $\sim4\times10^{13}$ p/cm^2, as for *RT* irradiation.

Experimental data on the pulse signal obtained for Si detectors and their analysis along with the treatment of the $Q_c(F)$ dependences using the Hecht equation were presented in [28]. It is clear from the results that nonequilibrium carriers generated by spills are captured by the radiation-induced deep level defects and change the electric field profile.

3.5. Heating at the final stage

At the final stage of the test the detectors were successively heated up, first to 80 K and then to *RT*. The changes in the detector characteristics after their heating up to 80 K were not significant. The dark current and the collected charge were at the same level as at 1.9 K. Only at $T>150$ K a significant signal recovery became noticeable in the silicon detectors (Fig. 11). During the final warm-up to *RT* the signal of the 10 kΩ cm silicon detector increased by a factor of 7.5 ± 1.2, compared to the one in liquid helium. The signal recovery started with the reappearance of a measurable dark current, indicating a link between the two effects.

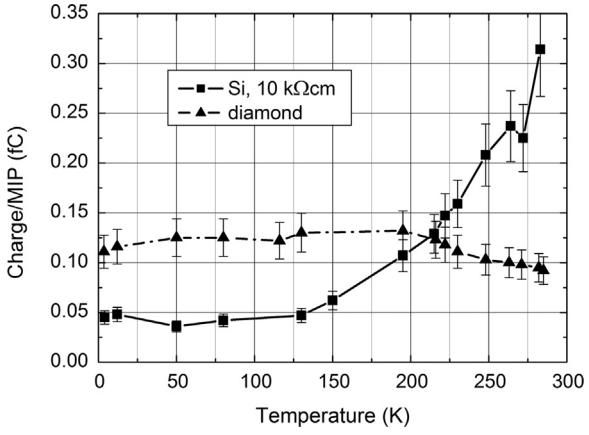

Fig. 11. Charge collected in silicon and diamond detectors irradiated to a fluence of 1.2×10^{16} p/cm^2 during the warm-up of the cryostat to *RT*.

Unlike this, the signal of the diamond detectors was less temperature-dependent than that of the silicon detectors and showed a small rise-decrease cycle during the heating. A smooth rise of the collected charge at low temperatures is not clear yet, while signal degradation above 200 K can be related to the reduction of the carrier mobility, which increases the charge collection time and, consequently, charge losses.

4. Summary

The first *in situ* long-term irradiation test of semiconductor detectors in a superfluid helium was performed at the CERN irradiation facility. The detectors based on silicon with different resistivity and single-crystal CVD diamond were irradiated to a final fluence of 1×10^{16} proton/cm^2, equivalent to a dose of about 2 MGy. At 1.9 K the dark current in the silicon detectors irradiated to a fluence above 5×10^{14} p/cm^2 decreased below 100 pA at 400 V even under forward bias, which was comparable to the current in the diamond detectors. The results of the irradiation test showed that both diamond and silicon detectors can operate at 1.9 K after 1×10^{16} p/cm^2 irradiation required for application as BLMs, whereas compliance with the conditions 4–6 listed in Section 1 can be tested only in further studies which are planned in the future.

The effect of radiation resulted in a decrease in the collected charge, and the $Q_c(F)$ dependences were obtained. The rate of the sensitivity degradation of Si detectors was controlled mainly by the operational mode, being larger at V_{forw}. Although the charge collected in the detectors operating at forward bias was larger at $F\leq(1–3)\times10^{15}$ p/cm^2, all Si detectors showed the same sensitivity (Q_c) after irradiation to 1×10^{16} p/cm^2. The degradation rate was larger in the silicon detectors than in the diamond ones, and at $F>(3–5)\times10^{15}$ p/cm^2 the charge collected in the diamond detectors was greater than Q_c in the Si detectors irrespective to the bias mode.

The negligible difference in the sensitivity of the detectors processed on silicon with various resistivity and irradiated to maximal fluence indicates the possibility of using silicon material with a resistivity lower than tens of kΩ cm, which can make the detector manufacturing cost-effective.

Acknowledgments

The work was performed within the framework of the Agreement on Scientific Collaboration between the CERN-BE-BI-BL group and the Ioffe Institute, and within the scope of the CERN-RD39 collaboration program. The study was supported in part by the Fundamental Program No 11P, project 3.2, of the Russian Academy of Sciences, Russia, on collaboration with CERN. The authors wish to express their deep gratitude to M. Glaser and F. Ravotti for performing the *in situ* irradiation and to the staff of the CERN Cryogenic Laboratory for their assistance in constructing the cryogenic system.

References

[1] A. Mereghetti, M. Sapinski, Fluka simulations for assessing thresholds of BLMS around the LHC triplet magnets, in: Proceedings of the Cryogenic Beam Loss Monitors Workshop, CERN, Geneva, Switzerland, October 2011, ⟨http://indico.cern.ch/event/CryoBLM2011⟩.
[2] ⟨www.cern.ch/rd50⟩.
[3] A. Affolder, et al., Nuclear Instruments and Methods in Physics Research Section A 658 (2011) 11.
[4] H. Jansen, D. Dobos, V. Eremin, H. Pernegger, N. Wermes, Physics Procedia 37 (2012) 2005.
[5] CIVIDEC Instrumentation, GmbH, Vienna, Austria; ⟨www.Cividec.at⟩.
[6] H. Frais-Kölbl, E. Griesmayer, H. Pernegger, H. Kagan, IEEE Transactions on Nuclear Science NS 51 (2004) 3833.
[7] E. Griesmayer, P. Kavrigin, Diamonds for beam instrumentation, in: Proceedings of the TIPP2014, Amsterdam, June 2-6, 2014, PoS (TIPP2014) 088, 2015, ⟨http://pos.sissa.it⟩.
[8] B. Dehning, et al., Overview of LHC Beam Loss Measurements, in: Proceedings of the IPAC2011, San Sebastian, Spain, September 4–9, 2011, p. 2854.
[9] B. Dehning, E. Effinger, D. Dobos, H. Pernegger, E. Griesmayer, Diamond beam loss monitors for LHC, ATS/Note/2011/048, 2011, ⟨http://cds.cern.ch/record⟩.
[10] C. Kurfürst, et al., Investigation of the use of silicon, diamond and liquid helium detectors for beam loss measurements at 2 K, in: Proceedings of the IPAC2012, New Orleans, USA, May, 2012, p. 1080.
[11] C. Kurfürst, Cryogenic Beam Loss Monitoring for the LHC (Dissertation), TU Wien, Geneva, 2013 (November).
[12] V.G. Palmieri, et al., Physica B 280 (2000) 532.
[13] G. Ruggiero, et al., Nuclear Instruments and Methods in Physics Research Section A 476 (2002) 583.
[14] G.D. Watkins, Defects and diffusion in silicon processing, in: T.D. De la Rubia, S. Coffa, P.A. Stolk, C.S. Rafferty (Eds.), Proceedings of the MRS Sypmosium, 469, Pittsburgh, 1997, p. 139.
[15] G.D. Watkins, Physics of Solid State 41 (1999) 746.
[16] M.R. Bartosik, et al., Characterisation of Si detectors for the use at 2 K, in: Proceedings of the IPAC 2013, Shanghai, China, May 12–17, 2013, pp. 643–645.
[17] C. Kurfuerst, et al., Operation of silicon, diamond and liquid helium detectors in the range of room temperature to 1.9 K and after an irradiation dose of several Mega Gray, in: Proceedings of the IBIC 2013, Oxford, UK, September 16–19 2013, pp. 791–794.
[18] C. Kurfuerst, et al., Radition tolerance of cryogenic beam loss monitor detectors, in: Proceedings of the IPAC2013, Shanghai, China, May 12–17, 2013, pp. 3240–3242.
[19] M. Glaser, L. Durieu, C. Leroy, M. Tavlet, P. Roy, F. Lemeilleur, Nuclear Instruments and Methods in Physics Research Section A 426 (1999) 72.
[20] F. Ravotti, M. Glaser, M. Moll, IEEE Transactions on Nuclear Science NS-53 (2006) 2016.
[21] V. Eremin, N. Strokan, E. Verbitskaya, Z. Li, Nuclear Instruments and Methods in Physics Research Section A 372 (1996) 388.
[22] V. Eremin, J. Härkönen, Z. Li, E. Verbitskaya, Nuclear Instruments and Methods in Physics Research Section A 583 (2007) 91.
[23] M. Lampert, P. Mark, Current Injection in Solids, Academic Press, London, NY, 1970.
[24] P. Siffert, et al., IEEE Transactions on Nuclear Science NS 23 (1976) 159.
[25] B. Dezillie, V. Eremin, Z. Li, E. Verbitskaya, Nuclear Instruments and Methods in Physics Research Section A 452 (2000) 440.
[26] G. Kramberger, V. Cindro, I. Mandić, M. Mikuž, M. Zavtranik, Nuclear Instruments and Methods in Physics Research Section A 476 (2002) 645.
[27] W. Adam, et al., Nuclear Instruments and Methods in Physics Research Section A 565 (2006) 278.
[28] E. Verbitskaya, et al., "Charge collection in Si detectors irradiated in-situ at superfluid helium temperature", pres. 10 Internat. Conf. "Radiation effects on semiconductor materials, detectors and devices" (RESMDD14), Oct 8-10, 2014, Florence.